25. Allender, D., Bray, J. & Bardeen, J. Model for an exciton mechanism of superconductivity. *Phys. Rev. B* **7,** 1020–1029 (1973).
26. Davis, D., Gutfreund, H. & Little, W. A. Proposed model of a high temperature excitonic superconductor. *Phys. Rev. B.* **13,** 4766–4779 (1976).
27. Hirsch, J. E. & Scalapino, D. J. Enhanced superconductivity in quasi two-dimensional systems. *Phys. Rev. Lett.* **56,** 2732–2735 (1986).
28. Bezryadin, A., Lau, C. N. & Tinkham, M. Quantum suppression of superconductivity in ultrathin nanowires. *Nature* **404,** 971–974 (2000).
29. Paquet, D., Rice, T. M. & Ueda, K. Two-dimensional electron-hole fluid in a strong perpendicular magnetic field: exciton Bose condensate or maximum density two-dimensional droplet. *Phys. Rev. B* **32,** 5208–5221 (1985).
30. Kellogg, M., Spielman, I. B., Eisenstein, J. P., Pfeiffer, L. N. & West, K. W. Observation of quantized Hall drag in a strongly correlated bilayer electron system. *Phys. Rev. Lett.* **88,** 126804 (2002).
31. Butov, L. V., Gossard, A. C. & Chemla, D. S. Macroscopically ordered state in an exciton system. *Nature* **418,** 751–754 (2002).
32. Snoke, S., Denev, S., Liu, Y., Pfeiffer, L. & West, K. Long-range transport in excitonic dark states in coupled quantum wells. *Nature* **418,** 754–757 (2002).

Acknowledgements We acknowledge discussions with E. Demler, H. Fertig, R. Gerhardts, W. Hanke, C. Kallin, M. Kruger, L. Manchanda, S. Mikhailov, A. Stern and M. Tinkham. This work has been supported by the ARO, BMBF, CSR at SRC, DFG and GIF.

Competing interests statement The authors declare that they have no competing financial interests.

Correspondence and requests for materials should be addressed to R.G.M. (e-mail: mani@deas.harvard.edu).

Wavelength-scalable hollow optical fibres with large photonic bandgaps for CO_2 laser transmission

Burak Temelkuran*, Shandon D. Hart*, Gilles Benoit, John D. Joannopoulos & Yoel Fink

Research Laboratory of Electronics and Department of Materials Science and Engineering, Massachusetts Institute of Technology, Cambridge, Massachusetts 02139, USA
** These authors contributed equally to this work*

Conventional solid-core optical fibres require highly transparent materials. Such materials have been difficult to identify owing to the fundamental limitations associated with the propagation of light through solids, such as absorption, scattering and nonlinear effects. Hollow optical fibres offer the potential to minimize the dependence of light transmission on fibre material transparency[1–3]. Here we report on the design and drawing of a hollow optical fibre lined with an interior omnidirectional dielectric mirror[4]. Confinement of light in the hollow core is provided by the large photonic bandgaps[5–7] established by the multiple alternating submicrometre-thick layers of a high-refractive-index glass and a low-refractive-index polymer. The fundamental and high-order transmission windows are determined by the layer dimensions and can be scaled from 0.75 to 10.6 μm in wavelength. Tens of metres of hollow photonic bandgap fibres for transmission of carbon dioxide laser light at 10.6 μm wavelength were drawn. The transmission losses are found to be less than 1.0 dB m^{-1}, orders of magnitude lower than those of the intrinsic fibre material, thus demonstrating that low attenuation can be achieved through structural design rather than high-transparency material selection.

Silica optical fibres[8,9] have been extremely successful in telecommunications applications, and other types of solid-core fibres have been explored at wavelengths where silica is not transparent[10,11]. However, all fibres that rely on light propagation principally through a solid material have certain fundamental limitations stemming from nonlinear effects, light absorption by electrons or phonons, material dispersion and Rayleigh scattering that limit maximum optical transmission power and increase attenuation losses[12,13]. These limitations have in turn motivated the study of a fundamentally different light-guiding methodology: the use of hollow waveguides having highly reflecting walls. Light propagation through air in a hollow fibre eliminates or greatly reduces the problems of nonlinearities, thermal lensing and end-reflections, facilitating high-power laser guidance and other applications that may be impossible using conventional fibres[12,14,15]. Hollow metallic or metallo-dielectric waveguides[12,16–19] have been studied fairly extensively and found useful practical applications, but their performance has been bounded by the notable losses occurring in metallic reflections at visible and infrared wavelengths, as well as by the limited length and mechanical flexibility of the fabricated waveguides. Hollow all-dielectric fibres relying on specular or attenuated total reflection have also been explored, but high transmission losses have prevented their broad application[12,20,21]. More recently, all-dielectric fibres consisting of a periodic array of air holes in silica have been used to guide light through air using narrow photonic bandgaps[1–3]. Solid-core, index guiding versions of these silica photonic crystal fibres have also been explored for applications such as very-large-core single-mode fibres, nonlinear enhancement and broadband supercontinuum generation, polarization maintenance and dispersion management[3]. However, the air-guiding capabilities of such waveguides have remained limited thus far by the difficulties in fabricating long, uniform fibres which must have a high volume fraction of air and many air–hole periods, as well as by the large electromagnetic penetration depths associated

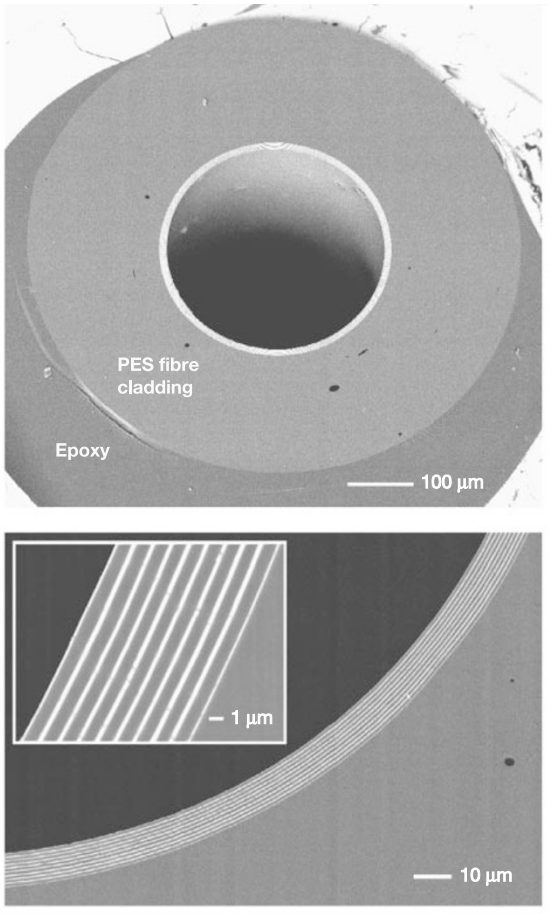

Figure 1 Cross-sectional SEM micrographs at various magnifications of hollow cylindrical multilayer fibre mounted in epoxy. The hollow core appears black, the PES layers and cladding grey, and the As_2Se_3 layers bright white. This fibre has a fundamental photonic bandgap at a wavelength of ~3.55 μm.

with the small photonic bandgaps achievable in these air–silica structures[2,22].

In the fibre we report here, the hollow core is surrounded by a solid multilayer structure of high refractive-index contrast, leading to large photonic bandgaps and omnidirectional reflectivity. The pertinent theoretical background[23] and recent analyses[24–27] indicate that such fibres may be able to achieve ultralow losses and other unique transmission properties (M. Ibanescu *et al.*, manuscript in preparation). The large photonic bandgaps result in very short electromagnetic penetration depths within the layer structure, significantly reducing radiation and absorption losses while increasing robustness.

To achieve high index contrast in the layered portion of the fibre, we combined a chalcogenide glass with a refractive index of ~2.8, arsenic triselenide (As_2Se_3), with a high glass-transition temperature thermoplastic polymer having a refractive index of ~1.55, poly(ether sulphone) (PES)[30]. We recently demonstrated that these materials could be thermally co-drawn into precisely layered structures without cracking or delamination, even under large temperature excursions[28]. The same polymer was used as a cladding material, resulting in fibres composed of ~98% polymer by volume (not including the hollow core); the fibres thus combine high optical performance with polymeric processability and mechanical flexibility. We fabricated a variety of fibres by depositing an As_2Se_3 layer (5–10 μm thick) by thermal evaporation onto a 25–50-μm-thick PES film, and the subsequent 'rolling' of that coated film into a hollow multilayer tube called a fibre pre-form. This hollow macroscopic pre-form was consolidated by heating under vacuum, and clad with a thick outer layer of PES; the layered pre-form was then placed in an optical fibre draw tower, and drawn down into tens or hundreds of metres of fibre having well-controlled submicrometre layer thicknesses. The nominal positions of the photonic bandgaps were determined by laser monitoring of the fibre outer diameter during the draw process. Typical standard deviations in the fibre outer diameter were ~1% of that diameter. The resulting fibres were designed to have large hollow cores, useful in high-energy transmission.

Scanning electron microscope (SEM) analysis (Fig. 1) reveals that the drawn fibres maintain proportionate layer thickness ratios, and that the PES and As_2Se_3 films adhere well during rigorous thermal cycling and elongation. Within the multilayer structure shown in Fig. 1, the PES layers (grey) have a thickness of 900 nm, and the As_2Se_3 layers (bright) are 270 nm thick (except for the first and last As_2Se_3 layers, which are 135 nm). Broadband fibre transmission spectra were measured with a Fourier-transform infrared (FTIR) spectrometer (Nicolet Magna 860), using a parabolic mirror to couple light into the fibre and an external detector. The results of these measurements are shown in Fig. 2, bottom panel, for fibres having two different layer structures. For each spectrum, light is guided at the fundamental and high-order photonic bandgaps. The top panel of Fig. 2 shows the corresponding photonic band diagram[4,7] for an infinite periodic multilayer structure, calculated using the experimental parameters of our fibre (layer thicknesses and indices). Good agreement is found between the positions of the measured transmission peaks and the calculated bandgaps, corroborated by the SEM-measured layer thicknesses, verifying that transmission is dominated by the photonic bandgap mechanism.

In order to demonstrate 'wavelength scalability' (that is, the control of transmission through the fibre's structural parameters), another fibre was produced having the same cross-section but with thinner layers. We compared the transmission spectrum of the original 3.55-μm-bandgap fibres with that of the fibre having scaled-down layer thicknesses. Figure 2 shows the shifting of the transmission bands, corresponding to fundamental and high-order photonic bandgaps, from one fibre to the next. The two fibres analysed in Fig. 2 were fabricated from the same fibre pre-form using different draw-down ratios (fibres with a fundamental bandgap centred near 3.55 μm have an outer diameter of 670 μm; those with a gap at 3.1 μm have an outer diameter of 600 μm). The high-order bandgaps are periodically spaced in frequency, as expected for such a photonic crystal structure. The fibre having a fundamental bandgap at 3.1 μm has a fourth-order bandgap at 775 nm (measured using a StellarNet EPP2000 spectrometer); this output from the hollow fibre core is imaged in Fig. 3 inset. Broadband light from a quartz–tungsten–halogen lamp was coupled into the 275-μm-diameter hollow core of the fibre shown in Fig. 3. Owing to the proximity of this wavelength to the electronic band edge of the As_2Se_3 glass, extra precautions were needed to reduce transmission due to glancing angle specular reflection. By placing multiple bends in the fibre, light transmitted owing to this effect was dramatically

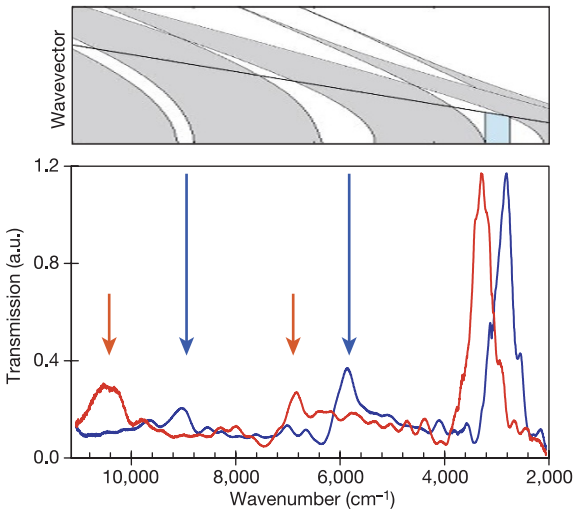

Figure 2 Photonic band structure due to the dielectric mirror, and the resulting transmission spectra for the hollow fibre. Upper panel, calculated photonic band structure associated with the dielectric mirror lining of the hollow fibre. Modes propagating through air and reflected by the fibre walls lie in the bandgaps (white) and within the light cone defined by the glancing-angle condition (black line). The grey regions represent modes radiating through the mirror. The fundamental bandgap has the widest range-to-midrange ratio, with a region of omnidirectional reflectivity highlighted in blue. Lower panel, comparison of transmission spectra for two different hollow fibres of ~30 cm length having similar structure but scaled photonic crystal (multilayer) period dimensions. The spectrum in blue is from a fibre with a fundamental photonic bandgap at 3.55 μm; the red spectrum is from a fibre where the corresponding bandgap is at 3.1 μm. High-order bandgaps (indicated by arrows) are periodically spaced in frequency.

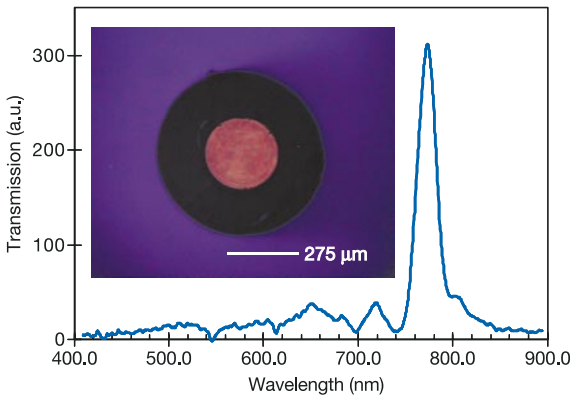

Figure 3 Visible to near-infrared transmission spectrum and charge-coupled device (CCD) image (inset) of light emerging from core of hollow fibre that has a fundamental bandgap at 3.1 μm. This fibre was ~25 cm long and bent multiple times. Imaged light is confined to the hollow core by the fourth-order photonic bandgap.

decreased. In short fibres (~30 cm), shallow bending was not found to greatly reduce transmission in the fundamental photonic bandgap, though bending losses in the high-order bandgaps are much greater. This should be expected, because the fundamental gap exhibits omnidirectional reflectivity while the high-order gaps do not. In order to qualitatively test the limits of this behaviour, a ~30-cm fibre having a bandgap at 3.55 μm was looped into a small 'knot' consisting of multiple bends (Fig. 4). Approximately 40% of the light in the fundamental bandgap was transmitted through this fibre when compared to the straight fibre, while the light guided in the high-order gaps was attenuated much more strongly. Hollow fibres with bandgaps near 3 μm are of interest for the transmission of high-energy Er:YAG laser radiation.

The wavelength scalability of our fibres was further demonstrated by the fabrication of hollow fibres designed for the transmission of 10.6-μm electromagnetic radiation. This not only shows that these structures can be made to guide light at extremely disparate wavelengths, but that specific bandgap wavelengths can be accurately targeted during fabrication and fibre drawing. Powerful and efficient CO_2 lasers are available that emit at 10.6 μm, and are used in such applications as laser surgery and materials processing, but waveguides operating at this wavelength have remained limited in length or loss levels[12,18]. Using the fabrication techniques outlined above, we produced fibres having hollow core diameters of 700–750 μm and outer diameters of 1,300–1,400 μm, with a fundamental photonic bandgap spanning the 10–11 μm wavelength regime, centred near 10.6 μm. Figure 5 depicts a typical FTIR transmission spectrum for these fibres, measured using ~30-cm-long straight fibres.

In order to quantify the transmission losses in these 10.6-μm-bandgap hollow fibres, fibre cutback measurements were performed. This involved the comparison of transmitted intensity through ~4 m of straight fibre with the intensity of transmission through the same section of fibre cut to shorter lengths (Fig. 5 inset). This test was performed on multiple sections of fibre, and the results found to be nearly identical for the different sections tested. The measurements were performed using a 25 W CO_2 laser (GEM-25, Coherent-DEOS) and high-power detectors (Newport 818T-10). The fibre was held straight; it was fixed at both ends, as well as at points near the middle to prevent variations in the input coupling and propagation conditions during fibre cutting. The laser beam was sent through focusing lenses as well as 500-μm-diameter pinhole apertures, and the input end face of the fibre was coated with a metal film to prevent accidental laser damage from misalignment (see Supplementary Information for further measurement details).

The transmission losses in the fundamental bandgap at 10.6 μm were measured to be 0.95 dB m^{-1}, as shown in the inset of Fig. 5, with an estimated measurement uncertainty of 0.15 dB m^{-1}. These loss measurements are comparable to some of the best reported loss values for other types of waveguides operating at 10.6 μm (refs 12, 29). A bending analysis for fibres with a bandgap centred at 10.6 μm revealed bending losses below 1.5 dB for 90° bends with bending radii from 4 to 10 cm (see Supplementary Information for further discussion of bending losses as well as modal considerations). We expect that these loss levels could be lowered even further by increasing the number of layers, through optimization of the layer thickness ratios and by creating a cylindrically symmetric multilayer fibre with no inner seam (present here because of the 'rolling' fabrication method). In addition, using a polymer with lower intrinsic losses should greatly improve the transmission characteristics.

One reasonable figure of merit for optical transmission losses through hollow all-dielectric photonic bandgap fibres is a comparison of the hollow fibre losses to the intrinsic losses of the materials used to make the fibre. As_2Se_3 has been explored as an infrared-transmitting material, yet the losses at 10.6 μm reported in the literature are ~7 dB m^{-1} for highly purified material, and more typically are greater than 10 dB m^{-1} for commercially available materials such as those used in our fabrication[29]. Based on FTIR transmission and spectroscopic ellipsometer measurements that we have performed on PES, the optical losses associated with propagation through solid PES should be greater than 100,000 dB m^{-1} at 10.6 μm. This demonstrates that guiding light through air in our hollow bandgap fibres leads to waveguide losses that are orders of magnitude lower than the intrinsic fibre material losses, which has been one of the primary goals of research into hollow photonic bandgap fibres. These comparatively low losses are made possible by the very short penetration depths of electromagnetic waves in the high-refractive-index-contrast photonic crystal structure, allowing these materials to be used at wavelengths that may have been thought improbable[18].

Another long-standing motivation of infrared fibre research has been the transmission of high-power laser light[11,19]. As a qualitative demonstration of the potential of our fibres for such applications, both straight and smoothly bent fibres of lengths 0.3 to 2.5 m were used to transmit sufficient CO_2 laser energy to burn holes in paper and a film of PES (the fibre majority component). This demonstrates the substantial reduction of fibre transmission loss relative to the intrinsic materials loss of the constituents (see Supplementary Information). The maximum laser power density coupled into our fibres in these trials was approximately 300 W cm^{-2}. No damage to

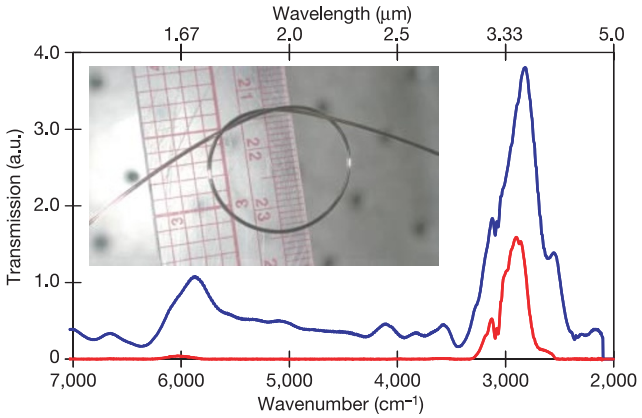

Figure 4 Transmission spectra for straight (blue) and 'knotted' (red) hollow fibre having a fundamental bandgap at 3.55 μm. The fibre knot consisted of multiple bends and the knot had a radius of ~1 cm (see inset). Approximately 40% of the light in the fundamental bandgap was transmitted through this highly perturbed fibre, whereas the high-order bandgap at 1.7 μm has much greater bending losses.

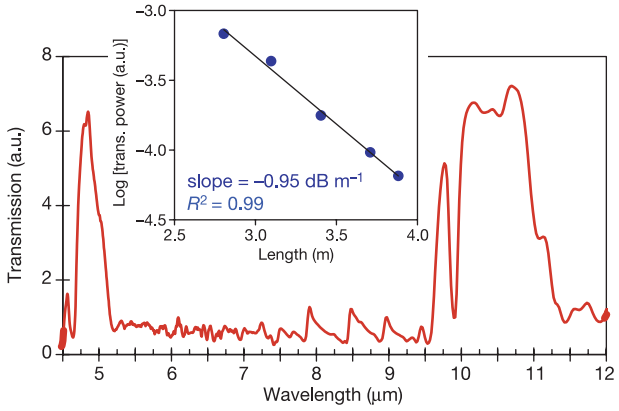

Figure 5 Typical transmission spectrum of hollow fibres designed to transmit CO_2 laser light. The fundamental photonic bandgap is centred near a wavelength of 10.6 μm, and the second-order gap is at ~5 μm. Inset, log(transmitted power) versus length of fibre. The slope of this graph is the loss in dB m^{-1}. The measured fibre has a hollow core diameter of 700 μm.

the fibres was observed when the laser beam was properly coupled into the hollow fibre core. These results indicate the feasibility of using hollow multilayer photonic bandgap fibres as a low-loss wavelength-scalable transmission medium for high-power laser light. □

Received 3 July; accepted 29 October 2002; doi:10.1038/nature01275.

1. Cregan, R. F. *et al.* Single-mode photonic band gap guidance of light in air. *Science* **285,** 1537–1539 (1999).
2. Allan, D. C. *et al. Photonic Crystals and Light Localization in the 21st Century* (ed. Soukoulis, C. M.) 305–320 (Kluwer, Boston, 2001).
3. Eggleton, B. J., Kerbage, C., Westbrook, P. S., Windeler, R. S. & Hale, A. Microstructured optical fiber devices. *Opt. Express* **9,** 698–713 (2001).
4. Fink, Y. *et al.* A dielectric omnidirectional reflector. *Science* **282,** 1679–1682 (1998).
5. Yablonovitch, E. Inhibited spontaneous emission in solid-state physics and electronics. *Phys. Rev. Lett.* **58,** 2059–2062 (1987).
6. John, S. Strong localization of photons in certain disordered dielectric superlattices. *Phys. Rev. Lett.* **58,** 2486–2489 (1987).
7. Joannopoulos, J. D., Meade, R. D. & Winn, J. N. *Photonic Crystals: Molding the Flow of Light* (Princeton Univ. Press, Princeton, New Jersey, 1995).
8. Maurer, R. D. & Schultz, P. C. US Patent 3,659,915 (1972).
9. Keck, D. B., Maurer, R. D. & Schultz, P. C. On the ultimate lower limit of attenuation in glass optical waveguides. *Appl. Phys. Lett.* **22,** 307–309 (1973).
10. Hilton, A. R. Optical properties of chalcogenide glasses. *J. Non-Cryst. Solids* **2,** 28–39 (1970).
11. Harrington, J. A. *Handbook of Optics* (ed. Bass, M.) 14.1–14.13 (McGraw-Hill, New York, 2001).
12. Harrington, J. A. A review of IR transmitting, hollow waveguides. *Fiber Integr. Opt.* **19,** 211–227 (2000).
13. Mitra, P. P. & Stark, J. B. Nonlinear limits to the information capacity of optical fibre communications. *Nature* **411,** 1027–1030 (2001).
14. Renn, M. J. *et al.* Laser-guided atoms in hollow-core optical fibers. *Phys. Rev. Lett.* **75,** 3253–3256 (1995).
15. Rundquist, A. *et al.* Phase-matched generation of coherent soft X-rays. *Science* **280,** 1412–1415 (1998).
16. Marcatilli, E. A. J. & Schmeltzer, R. A. Hollow metallic and dielectric waveguides for long distance optical transmission and lasers. *Bell Syst. Tech. J.* **43,** 1783–1809 (1964).
17. Miyagi, M. & Kawakami, S. Design theory of dielectric-coated circular metallic waveguides for infrared transmission. *J. Lightwave Technol.* **2,** 116–126 (1984).
18. Matsuura, Y., Kasahara, R., Katagiri, T. & Miyagi, M. Hollow infrared fibers fabricated by glass-drawing technique. *Opt. Express* **10,** 488–492 (2002).
19. Hongo, A., Morosawa, K., Matsumoto, K., Shiota, T. & Hashimoto, T. Transmission of kilowatt-class CO_2-laser light through dielectric-coated metallic hollow wave-guides for material processing. *Appl. Opt.* **31,** 5114–5120 (1992).
20. Bornstein, A. & Croitoru, N. Chalcogenide hollow fibers. *J. Non-cryst. Solids* **77–78,** 1277–1280 (1985).
21. Fitt, A. D., Furusawa, K., Monro, T. M. & Please, C. P. Modeling the fabrication of hollow fibers: Capillary drawing. *J. Lightwave Technol.* **19,** 1924–1931 (2001).
22. Broeng, J., Barkou, S. E., Søndergaard, T. & Bjarklev, A. Analysis of air-guiding photonic bandgap fibers. *Opt. Lett.* **25,** 96–98 (2000).
23. Yeh, P., Yariv, A. & Marom, E. Theory of Bragg fiber. *J. Opt. Soc. Am.* **68,** 1196–1201 (1978).
24. Ouyang, G., Xu, Y. & Yariv, A. Comparative study of air-core and coaxial Bragg fibers: single-mode transmission and dispersion characteristics. *Opt. Express* **9,** 733–747 (2001).
25. Ibanescu, M., Fink, Y., Fan, S., Thomas, E. L. & Joannopoulos, J. D. An all-dielectric coaxial waveguide. *Science* **289,** 415–419 (2000).
26. Johnson, S. G. *et al.* Low-loss asymptotically single-mode propagation in large-core OmniGuide fibers. *Opt. Express* **9,** 748–779 (2001).
27. Fink, Y. *et al.* Guiding optical light in air using an all-dielectric structure. *J. Lightwave Technol.* **17,** 2039–2041 (1999).
28. Hart, S. D. *et al.* External reflection from omnidirectional dielectric mirror fibers. *Science* **296,** 510–513 (2002).
29. Sanghera, J. S. & Aggarwal, I. D. Active and passive chalcogenide glass optical fibers for IR applications: a review. *J. Non-cryst. Solids* **257,** 6–16 (1999).
30. Bormashenko, E., Pogreb, R., Pogreb, Z. & Sutovski, S. Development of new near-infrared filters based on the "sandwich" polymer-chalcogenide glass-polymer composites. *Opt. Eng.* **40,** 661–662 (2001).

Supplementary Information accompanies the paper on *Nature*'s website (http://www.nature.com/nature).

Acknowledgements We thank P. H. Prideaux for teaching us the ways and means of optical fibre drawing; G. R. Maskaly, H. Burch, K. R. Maskaly, E. P. Chan, O. Shapira, M. Bayindir, C. H. Sarantos and C. Guaqueta for their contributions;. L. H. Galindo, T. McClure and M. Frongillo for experimental aid; W. A. King, J. A. Harrington, A. R. Hilton, E. L. Thomas, U. Kolodny and R. Stata for discussions and support; L. Laughman, L. Newman, A. DeMaria and the team at Coherent-DEOS for assistance; and W. H. Smith, M. Young and the MIT-RLE for administrative support. This work was supported in part by DARPA-QUIST/ARO, the NSF, the US DOE, and an NSF graduate research fellowship (S.D.H.). This work was also supported by the Materials Research Science and Engineering Center (MRSEC) programme of the NSF, and made use of MRSEC shared facilities.

Competing interests statement The authors decline to provide information about competing financial interests.

Correspondence and requests for materials should be addressed to Y.F. (e-mail: yoel@mit.edu).

Bond-controlled configurational entropy reduction in chemical vitrification

Silvia Corezzi*, Daniele Fioretto* & Pierangelo Rolla†

** Istituto Nazionale per la Fisica della Materia and Dipartimento di Fisica, Università di Perugia, Via A. Pascoli, I-06123, Perugia, Italy*
† Istituto Nazionale per la Fisica della Materia and Dipartimento di Fisica, Università di Pisa, Via F. Buonarroti 2, I-56127, Pisa, Italy

Glass formation is usually viewed in terms of physical vitrification: a liquid in a metastable state[1] is cooled or compressed so as to avoid crystallization. However, glasses may also be formed by chemical vitrification, a process involving progressive polymerization of the constituent molecules via the formation of irreversible chemical bonds. The formation of most of the materials used in engineering plastics and the hardening of natural and synthetic resins are based on chemical vitrification. Despite the differences in the molecular processes involved in chemical and physical vitrification, surprising similarities[2–9] are observed in the slowing down of the dynamics and in the thermodynamical properties of the resulting glasses. Explaining such similarities would improve general understanding of the glass transition and may disclose its universal nature. Here we report dielectric and photon-correlation measurements that reveal the origin of the similarity in the dynamical behaviour of physical and chemical glass formers. We find that the evolution of their configurational restrictions proceeds in a similar manner. In particular, we make a connection between the reduction in configurational entropy and the number of chemical bonds, a quantity that can be controlled in experiments.

The polymerization of liquid monomers is an irreversible process that modifies molecular motions in reacting systems in a manner that closely resembles the reversible effect of reducing temperature or increasing pressure in chemically stable glass-forming liquids, and ultimately leads to a 'jammed' structure. However, glass science has mainly focused on glasses obtained following changes of temperature and pressure, called here the 'physical' glasses. No comparable effort has been made to clarify how microscopic processes of a chemical nature can result in a similar state of matter. In principle, there exists the possibility that physical and chemical vitrification have nothing in common apart from the final state. We show here that this is not the case.

In physical glasses, the dynamics of liquids approaching the glass transition strongly reflect the underlying thermodynamics of the liquid state. One way of rationalizing this qualitative notion is in terms of the Adam–Gibbs theory[10], establishing a link between the structural relaxation time τ (a dynamic quantity) and the configurational entropy S_c (a thermodynamic quantity) of a liquid, in the form

$$\tau = \tau_0 \exp(C/TS_c) \qquad (1)$$

with τ_0 and C nearly constant. The fundamental outcome as given by equation (1) appears to be preserved by modern treatments[11] of entropy-based theories. Indeed, the extent to which results of experimental studies performed by varying temperature[12] and pressure[13,14] agree with equation (1) is surprising; results of computer simulations performed at different temperatures and densities[15,16] on model glass formers similarly agree with equation (1). This agreement goes beyond what would be expected from a naïve model, as any entropy theory seems to be. It is now our aim to show that chemical vitrification shares with physical vitrification the same fundamental interpretation.